Electronic structure of layered transition-metal dichalcogenides $Nb_{1-x}Ti_xXc_2$ (Xc = S, Se, Te) studied by angle-resolved photoemission spectroscopy

2004 J. Phys.: Condens. Matter 16 8599

(http://iopscience.iop.org/0953-8984/16/47/012)

INSTITUTE OF PHYSICS PUBLISHING JOURNAL OF PHYSICS: CONDENSED MATTER

J. Phys.: Condens. Matter **16** (2004) 8599–8608 PII: S0953-8984(04)83532-X

Electronic structure of layered transition-metal dichalcogenides $Nb_{1-x}Ti_xXc_2$ (Xc = S, Se, Te) studied by angle-resolved photoemission spectroscopy

T Sato[1,3], **H Komatsu**[1], **K Terashima**[1], **T Takahashi**[1], **M Shimakawa**[2] **and K Hayashi**[2]

[1] Department of Physics, Tohoku University, Sendai 980-8578, Japan
[2] Okayama University of Science, 1-1 Ridai-cho, Okayama 700-0005, Japan

Received 8 July 2004, in final form 28 October 2004
Published 12 November 2004
Online at stacks.iop.org/JPhysCM/16/8599
doi:10.1088/0953-8984/16/47/012

Abstract

We have performed systematic high-resolution angle-resolved photoemission spectroscopy (ARPES) on layered transition-metal dichalcogenides $Nb_{1-x}Ti_xXc_2$ (Xc = S, Se, Te) to study the mechanism of metal–semiconductor transition as a function of x and Xc. We found a pseudogap near E_F in the S- and Se-based compounds while a clear Fermi edge is observed in the Te-based compound. The existence of the pseudogap indicates the strong scattering of electrons by the random potential caused by substitution, which prevents formation of the charge density wave and at the same time decreases the metallic conductivity. The metallic character of $Nb_{1-x}Ti_xTe_2$ is explained in terms of the relatively strong Te 5p–Nb 4d (Ti 3d) hybridization near E_F.

1. Introduction

Layered transition metal dichalcogenides (MXc_2, where M is the transition metal and Xc the chalcogen atom) have attracted much attention because of their unique electronic properties such as a variety of charge density wave (CDW) and superconducting transitions. In many MXc_2s, Nb and Ti dichalcogenides have drawn a considerable interest. Angle-resolved photoemission spectroscopy (ARPES) has yielded an important insight into the mechanism of their CDW and superconductivity by elucidating the band structure, the Fermi surface (FS), and the CDW/superconducting energy gap in 2H-$NbSe_2$ [1, 2], 1T-$TiSe_2$ [3], and 1T-$TiTe_2$ [4–6]. The mechanism of the characteristic CDW transition has been argued not only in terms of the conventional Fermi-surface (FS) nesting, but also by other exotic models such as the saddle point model [7], the excitonic insulator model [8, 9], and the Jahn–Teller distortion [10].

[3] Author to whom any correspondence should be addressed.

There has been intensive discussion from the lineshape analysis of ARPES spectra of whether 1T-$TiTe_2$ can be regarded as a typical Fermi liquid or not [4–6].

It has been reported that alloying between $NbXc_2$ and $TiXc_2$ causes quite interesting physical properties which are absent in both end materials. It is well known that 2H-NbS_2 shows superconductivity at 6.3 K while TiS_2 is semimetallic, and both show no CDW signature. By substituting a small amount (10%) of Ti for Nb in NbS_2, the compound becomes semiconductive [11]. The semiconducting nature persists up to $x = 0.9$ in $Nb_{1-x}Ti_xS_2$ with the largest resistivity value at around $x = 0.4$ [11]. The ground state of $NbSe_2$ ($TiSe_2$) is known to be the incommensurate (commensurate) CDW state. On substitution of Nb (20%) for Ti in $TiSe_2$, the CDW-induced anomaly in the resistivity rapidly disappears, showing a distinct semiconducting behaviour similar to $Nb_{1-x}Ti_xS_2$ [12]. In contrast to the semiconducting nature of S- and Se-based compounds, the electrical resistivity of Te-based $Nb_{1-x}Ti_xTe_2$ shows an anomalous temperature-independent 'nearly metallic' behaviour irrespective of the substitution content x [12], while the parent compounds, $NbTe_2$ and $TiTe_2$, are a superconductor ($T_c = 0.5$ K) and a semimetal, respectively. These reports show that there are two different types of 'metal'–semiconductor transitions in $Nb_{1-x}Ti_xXc_2$ (Xc = S, Se, Te); one is due to the substitution of transition metals and the other is due to replacement of chalcogen atoms. However, the microscopic origin for the transition has not been fully understood because of lack of experimental input on the detailed electronic band structure, in particular near the Fermi level (E_F).

In this paper, we report high-resolution ARPES on $Nb_{1-x}Ti_xXc_2$ (Xc = S, Se, Te) to study the mechanism of the metal–semiconductor transition. We found that the gross feature of valence band structure shows a good agreement between the ARPES experiment and the band calculations for $NbXc_2$ and $TiXc_2$. We observed a strong suppression in the spectral intensity near E_F (pseudogap) in the S- and Se-based compounds, while the Te-based compound shows a metallic Fermi edge. We discuss these differences in terms of the impurity scattering by substitution and the hybridization strength between the chalcogen p and the transition metal d band.

2. Experiments

Single crystals of $Nb_{1-x}Ti_xXc_2$ were prepared by the chemical-vapour transport method [11]. A quartz ampoule which contains starting materials (Ti powder, Nb powder, and Xc blocks) was heated at 1000–1100 °C for 2 days, annealed for one week, and then quenched in water [11]. In the present study, we prepared three different compounds, $Nb_{0.6}Ti_{0.4}S_2$, $Nb_{0.2}Ti_{0.8}Se_2$, and $Nb_{0.6}Ti_{0.4}Te_2$. The powder x-ray patterns show that all of these compounds have a 1T-type structure (figure 1(a))[12]. The resistivity of $Nb_{0.6}Ti_{0.4}S_2$ and $Nb_{0.2}Ti_{0.8}Se_2$ shows semiconducting behaviour while that of $Nb_{0.6}Ti_{0.4}Te_2$ is less temperature dependent (figure 1(b)).

ARPES measurements were performed using a Gammadata-Scienta SES-200 spectrometer with a high-flux discharge lamp and a toroidal grating monochromator. The He Iα ($h\nu = 21.218$ eV [13]) resonance line was used to excite photoelectrons. The energy and angular (momentum) resolutions were set at 15 meV and 0.2° (0.007 Å^{-1}), respectively. A clean surface for ARPES measurements was obtained by *in situ* cleaving of a crystal in an ultrahigh vacuum better than 3×10^{-11} Torr. We measured ARPES spectra within 24 h after cleaving, during which we did not observe any significant changes in the spectra indicative of the contamination/degradation of the sample surface. The Fermi level (E_F) of the sample was referenced to that of a gold film evaporated onto the sample substrate.

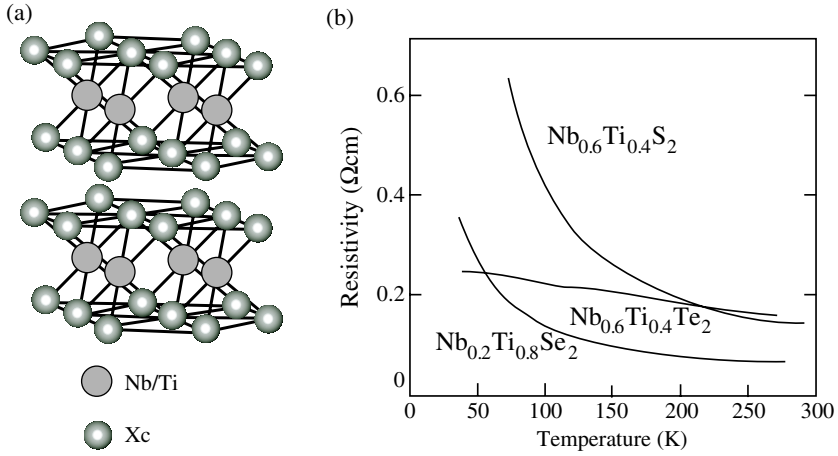

Figure 1. (a) Crystal structure and (b) temperature dependence of the electrical resistivity of $Nb_{1-x}Ti_xXc_2$ (Xc = S, Se, Te).

3. Results and discussion

3.1. Electronic structure of $Nb_{0.6}Ti_{0.4}S_2$

Figures 2(a) and (b) show angle-resolved photoemission spectra of $Nb_{0.6}Ti_{0.4}S_2$ measured at 30 K along the ΓM(AL) and ΓK(AH) directions, respectively. We find several dispersive peaks in the spectra for both directions. The overall dispersive feature of peaks appears to be similar in both directions around the Γ(A) point, while the difference becomes remarkable on going to the Brillouin-zone boundary, M(L) and K(H) points. According to the band calculations [14, 15], a dispersive band having the bottom at 1 eV near the M(L) point is ascribed to admixture of the Ti 3d and Nb 4d states, while other bands at higher binding energies are assigned to the S 3p bands. In order to see more clearly the dispersive feature of bands in the ARPES spectra, we have mapped out the 'band structure' and show the result in figures 2(c) and (d). The experimental band structure has been obtained by taking the second derivative of the ARPES spectra and plotting the intensity with a grey scale as a function of the wavevector and binding energy. Bright areas correspond to the experimental bands. Self-consistent linear-combination-of-atomic-orbital (LCAO) band calculation for TiS_2 [14] is shown by solid and dashed curves for comparison. As seen in figures 2(c) and (d), the overall valence-band structure shows a good agreement between the experiment and the calculation, demonstrating that the band structure calculation of TiS_2 serves as a good starting point to describe the electronic structure of $Nb_{1-x}Ti_xS_2$. In spite of the overall good agreement between the experiment and the calculation, we find two characteristic differences. The first is the energy position of a band close to E_F; the bottom of the band at M(L) point is located at 0.7 eV from E_F while that of the band calculation is at 0.3 eV. The difference may originate in the chemical potential shift by the substitution of Nb with an excess electron in a unit cell. As discussed later, formation of a 'pseudogap' at E_F may also be responsible for this energy difference. The second is that a band at 2 eV around the Γ(A) point is absent in the calculation. This feature is explained by taking into account the band structure of Nb dichalcogenide. We will discuss this point later [15].

Figures 3(a) and (b) show the high-resolution ARPES spectra near E_F of $Nb_{0.6}Ti_{0.4}S_2$ measured at 30 K along the ΓM(AL) and ΓK(AH) directions, respectively. The ARPES-

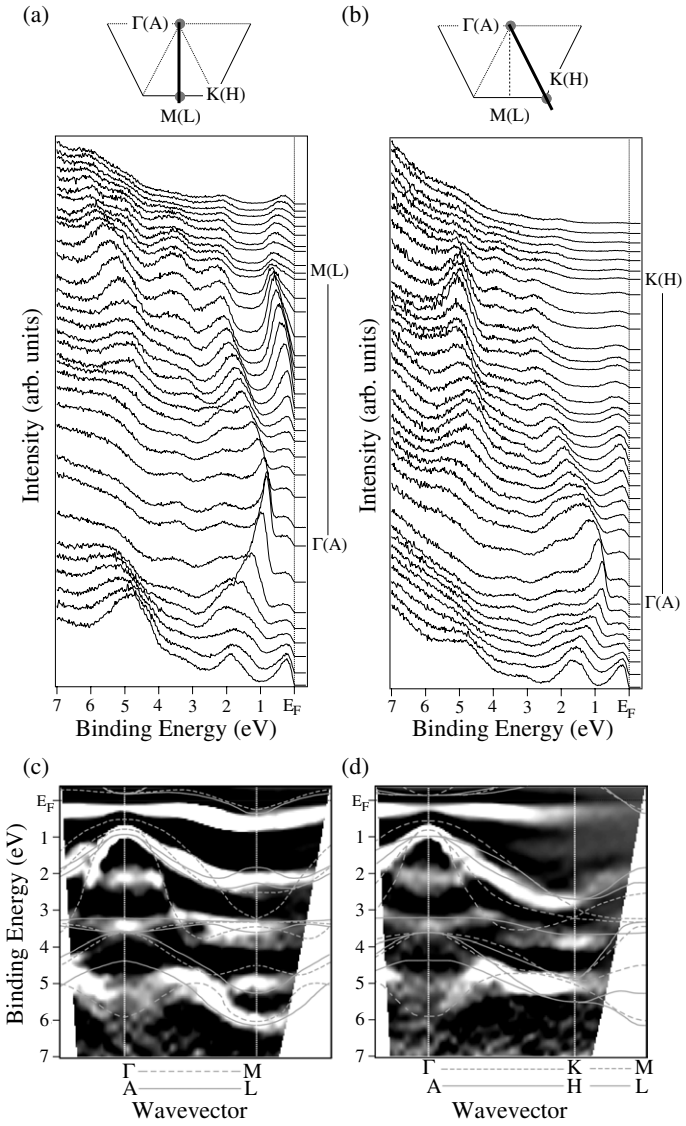

Figure 2. Valence-band ARPES spectra of $Nb_{0.6}Ti_{0.4}S_2$ measured at 30 K with the He Iα resonance line along (a) ΓM(AL) and (b) ΓK(AH) directions. Experimentally determined valence-band structure of $Nb_{0.6}Ti_{0.4}S_2$ along (c) ΓM(AL) and (d) ΓK(AH) directions, compared with the LCAO band calculation for TiS_2 [14].

intensity plot is shown in figures 3(c) and (d). We find in figures 3(a) and (b) that two bands disperse near E_F in the ΓM(AL) direction. The first band has the top of energy dispersion at 0.9 eV below E_F at the Γ(A) point and steeply disperses toward the high binding energy on going to the M(L) point. The second one appears at E_F midway between Γ(A) and M(L) points, and shows a relatively slow dispersion toward the zone boundary. The first band is assigned to the S 3p states, while the second one is attributed to the Nb 4d–Ti 3d mixed states. It is clear from figures 3(a) and (c) that although the band close to E_F suddenly loses its intensity midway between Γ(A) and M(L) points as if the band crosses E_F, the band actually

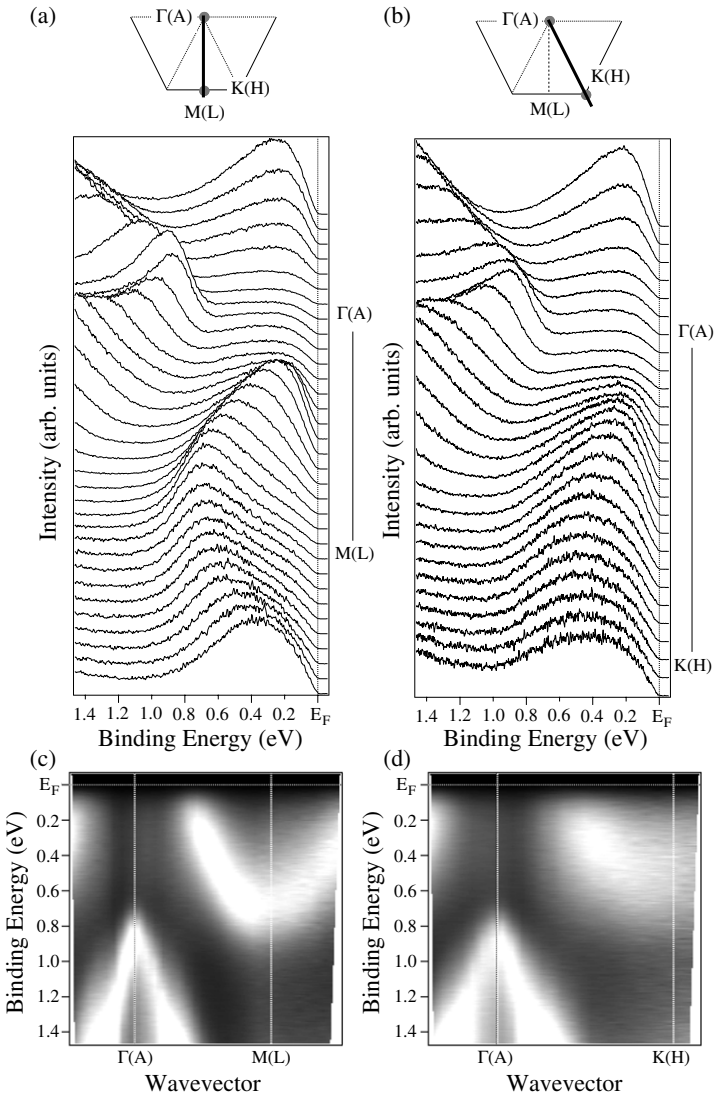

Figure 3. ARPES spectra in the vicinity of E_F of $Nb_{0.6}Ti_{0.4}S_2$ measured at 30 K along (a) ΓM(AL) and (b) ΓK(AH) directions. The ARPES-intensity plot as a function of momentum and binding energy is shown in (c) and (d).

does not cross E_F because the leading-edge midpoint of the spectra is apparently about 0.1 eV away from E_F in the whole momentum range. The leading-edge shift together with the strong suppression of the spectral weight in the vicinity of E_F, namely formation of a 'pseudogap', is also seen in the ΓK(AH) direction (figures 3(b) and (d)). This 'pseudogap' is different from a real 'gap' since ARPES spectra in the vicinity of E_F show a characteristic tail which extends very close to E_F with finite spectral weight around E_F, which is different from the behaviour of a real 'gap', where we expect to observe the shift in the leading-edge starting point toward higher binding energy with negligible spectral weight around E_F. There are four possible scenarios to explain this pseudogap: (i) CDW gap, (ii) normal bandgap, (iii) correlation gap,

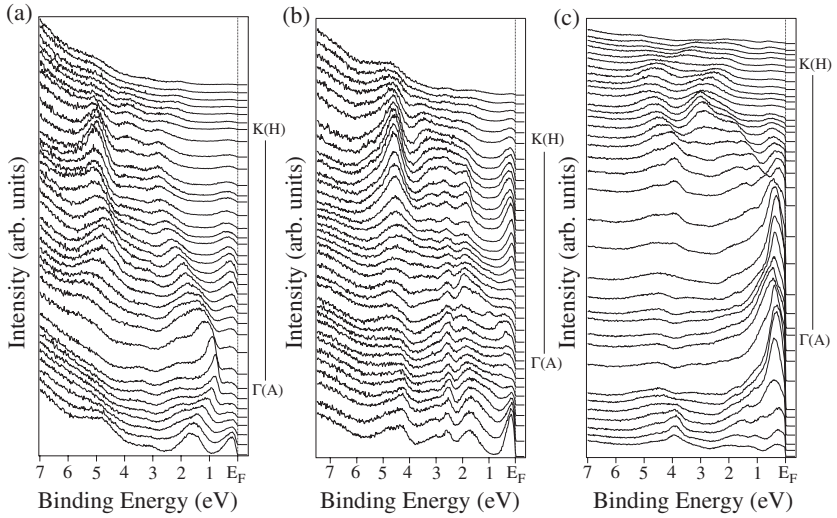

Figure 4. Comparison of valence-band ARPES spectra along ΓK(AH) direction in (a) $Nb_{0.6}Ti_{0.4}S_2$, (b) $Nb_{0.2}Ti_{0.8}Se_2$, and (c) $Nb_{0.6}Ti_{0.4}Te_2$.

and (iv) disorder/randomness-induced coulomb gap. Absence of the CDW-induced anomaly in the electrical resistivity as seen in figure 1(b) obviously contradicts scenario (i). This is also consistent with the experimental fact that both end materials NbS_2 and TiS_2 do not show any signature of CDW transition. Furthermore, in the case of (i), we expect folding of the band as seen in other CDW compounds [16]. However, as clearly seen from figure 3(c), we do not observe any dispersing-back behaviour as we approach the Γ(A) point from midway between the M(L) and Γ(A) point. This obviously contradicts scenario (i). In the case of (ii), the band closest to E_F should appear in the whole momentum range since the band has to be fully occupied. This is not seen in the present ARPES result since the spectral weight near E_F around the Γ(A) point is very small as compared to that around the M(L) point. In the case of (iii), we should observe the relatively large spectral weight around the Γ(A) point together with the dispersing-back behaviour of the band, as observed in the parent compounds of cuprate high-temperature superconductors [17]. Furthermore, the overall good agreement of the band dispersion between the experiment and the band calculation indicates less importance of the electron correlation, which is not in favour of the opening of a large correlation gap. Therefore, scenario (iv) is most probable to explain the observed pseudogap. It is inferred that the random potential induced by substitution causes a strong scattering of electrons and at the same time degrades the coherence among electrons near E_F [18], leading to opening of a pseudogap at E_F.

3.2. Chalcogen dependence of electronic structure

Figure 4 shows valence-band ARPES spectra of $Nb_{1-x}Ti_xXc_2$ (Xc = S, Se, Te) measured along the ΓK(AH) direction. We clearly find that each compound shares several common features, for example, a dispersionless weak feature in the vicinity of E_F at around the K(H) point and several dispersive bands at higher binding energies. We also find a systematic change in the energy dispersion of the hole-like band centred at the Γ(A) point when we change the chalcogen atom from S to Te. The top of dispersion at the Γ(A) point is located about 0.8 eV

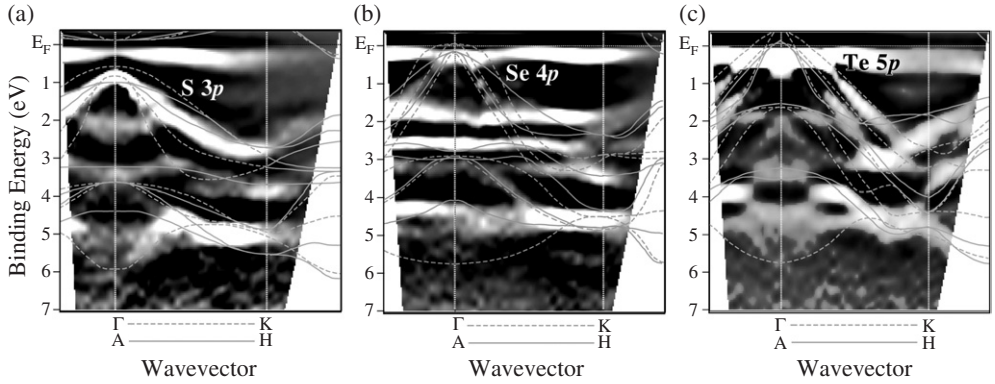

Figure 5. Comparison of experimentally determined valence-band structure in (a) $Nb_{0.6}Ti_{0.4}S_2$, (b) $Nb_{0.2}Ti_{0.8}Se_2$, and (c) $Nb_{0.6}Ti_{0.4}Te_2$. Band calculations of TiS_2 [14], $TiSe_2$ [19], and $TiTe_2$ [20] are superimposed by dashed and solid curves.

away from E_F in the sulfide, being almost on E_F in the selenide, and finally goes above E_F in the telluride.

In order to see the change in the electronic structure as a function of Xc in more detail, we have mapped out the band structure of each compound and compare with the band structure calculation for $TiXc_2$ [14, 19, 20] in figure 5. We find that the overall feature of band structure shows a good agreement between the experiment and the calculation. By comparing with the calculation, the observed hole-like band is assigned to the chalcogen p band. The systematic energy shift of the chalcogen p band toward E_F in the experiment is well reproduced in the calculation. However, a finite intensity just below E_F around the K(H) point in the experiment is not reproduced in the calculation for $TiXc_2$, suggesting that this feature may originate in the Nb 4d band.

To clarify this point, we show in figure 6 the comparison of the experimental band structure of $Nb_{0.2}Ti_{0.8}Se_2$ with the band calculation for both $TiSe_2$ [19] and $NbSe_2$ [21]. We find that several experimental bands which do not have a counterpart in the band calculation for $TiSe_2$ are well reproduced in the calculation for $NbSe_2$. For example, an experimental flat band observed at 1.8 eV in the ΓK(AH) direction has no theoretical counterpart in the calculation for $TiSe_2$ (figure 6(a)), but is well reproduced in the calculation for $NbSe_2$ (figure 6(b)). A finite intensity just below E_F around the K(H) point in the experiment is totally missing in the calculation for $TiSe_2$, while a corresponding feature is found in the calculation for $NbSe_2$, although the momentum region where the band appears below E_F is different. The good correspondence of a finite intensity just below E_F to the calculated bands in $NbSe_2$ is more clearly seen along the ΓM(AL) direction. We find in figure 6(d) that not only the energy position but also the momentum region of the band show a good agreement, while the calculation of $TiSe_2$ does not reproduce satisfactorily the experimental result. We think that the relatively poor agreement between the experiment and the calculation of $NbSe_2$ near the K(H) point (figure 6(b)) may be due to a strong scattering effect; the Nb-4d-derived band, which exists around the M(L) point, suffers a strong scattering by phonons so that an incoherent-type broad feature may also appear around the K(H) point.

To see more clearly the change in the electronic structure near E_F as a function of Xc, we show in figure 7 ARPES spectra near E_F of the ΓK(AH) direction for three compounds. We clearly find a systematic shift of the chalcogen p band around the Γ(A) point toward

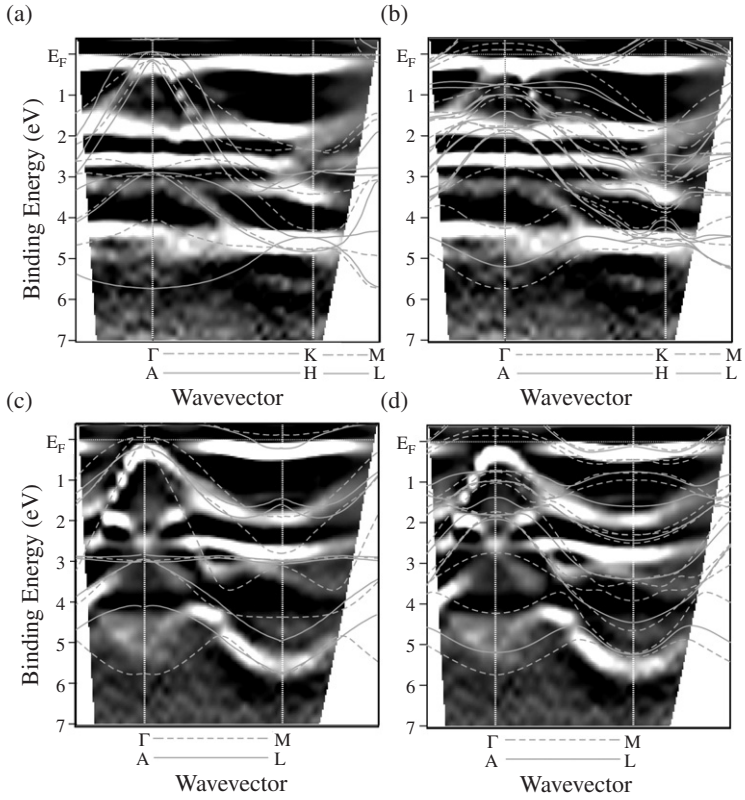

Figure 6. Comparison of the experimentally determined valence-band structure of $Nb_{0.2}Ti_{0.8}Se_2$ along the ΓK(AH) direction with the band calculation for (a) $TiSe_2$ [19] and (b) $NbSe_2$ [21]. The same along the ΓM(AL) direction for (c) $TiSe_2$ and (d) $NbSe_2$.

E_F when we change the chalcogen from S to Te. It is remarked that although leading-edge shift is clearly observed in $Nb_{0.2}Ti_{0.8}Se_2$, the energy shift relative to E_F is smaller than that in $Nb_{0.6}Ti_{0.4}S_2$. In sharp contrast to the semiconducting behaviour of the S- and Se-based compounds, $Nb_{0.6}Ti_{0.4}Te_2$ shows a distinct Fermi-edge cut-off indicative of the intrinsic metallic nature. Since the scattering potential between $Nb_{0.6}Ti_{0.4}S_2$ and $Nb_{0.6}Ti_{0.4}Te_2$ is thought to be similar because the substitution content ($x = 0.4$) is the same in both compounds, the difference in the electrical property (semiconducting or metallic) would be attributed to the band structure itself, especially the hybridization strength between the chalcogen p band and the transition metal d band. Since the Te 5p band crosses E_F in $Nb_{0.6}Ti_{0.4}Te_2$ and produces a hole pocket at the Γ(A) point as seen in figure 7(c), the d band should be shifted downward across E_F to keep the charge neutrality. In fact, a new feature probably due to the d band appears at 0.7 eV around the K(H) point in $Nb_{0.6}Ti_{0.4}Te_2$ although the d band gradually moves toward E_F on going from the sulfide to the selenide. It is expected that the overlapping of the energy range between the Te 5p and the Nb 4d (Ti 3d) states around E_F enhances the hybridization between the two bands. This leads to a larger band width as well as the larger Fermi velocity and reduces the importance of scattering, giving rise to the high density of states (DOS) at E_F, so that the random potential by substitution is not strong enough to remove all the states at E_F, leaving a finite DOS at E_F. This remaining DOS at E_F would therefore be

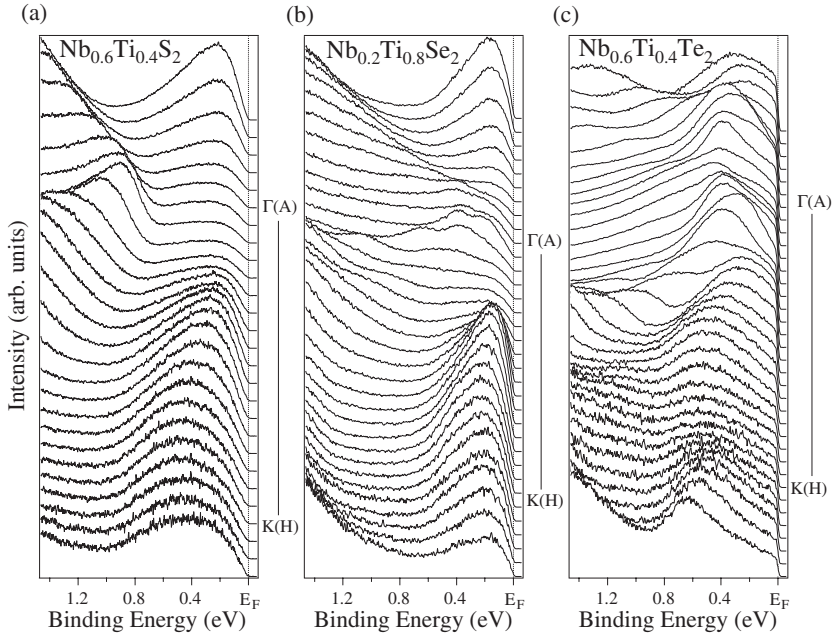

Figure 7. Comparison of ARPES spectra in the vicinity of E_F in (a) $Nb_{0.6}Ti_{0.4}S_2$, (b) $Nb_{0.2}Ti_{0.8}Se_2$, and (c) $Nb_{0.6}Ti_{0.4}Te_2$.

responsible for the metallic character of $Nb_{0.6}Ti_{0.4}Te_2$. All these experimental facts suggest that the semiconductor–metal transition in $Nb_{1-x}Ti_xXc_2$ as a function of Xc is characterized by the strength of the p–d hybridization strength, while that as a function of x is dominated by the strength of random potential caused by the substitution of Nb for Ti.

4. Summary

We have performed high-resolution angle-resolved photoemission spectroscopy on $Nb_{1-x}Ti_xXc_2$ (Xc = S, Se, Te) to study the metal–semiconductor transition caused by substitution of the transition metal as well as by replacement of the chalcogen atom. We have determined the band structure of all the valence states as well as that near E_F more precisely. The gross feature of the experimentally determined band structure is well explained by the band structure calculations of Nb and Ti dichalcigenide. In the transition-metal-substituted sulfide and selenide, we found a pseudogap at E_F, reflecting the semiconducting nature of the compounds. It is inferred that the pseudogap with almost no DOS at E_F is produced by the random potential by the substitution. In contrast, a finite DOS at E_F indicative of metallic nature is observed in the telluride. The experimentally determined band structure of the telluride shows that there is a large energy overlap between the Te 5p and the Nb 4d (Ti 3d) states near E_F. This leads to the higher DOS at E_F as well as larger Fermi velocity, reducing the importance of scattering, and therefore responsible for the metal–semiconductor transition as a function of Xc.

Acknowledgment

This work is supported by a grant from the MEXT of Japan.

References

[1] Yokoya T, Kiss T, Chainani A, Shin S, Nohara M and Takagi H 2001 *Science* **294** 2518
[2] Valla T, Fedorov A V, Johnson P D, Glans P-A, McGuinness G, Smith K E, Andrei E Y and Berger H 2004 *Phys. Rev. Lett.* **92** 186401
[3] Kidd T E, Miller T, Chou M Y and Chiang T-C 2002 *Phys. Rev. Lett.* **88** 226402
[4] Claessen R, Anderson R O, Gweon G-H, Allen J W, Ellis W P, Janowitz C, Olson C G, Shen Z X, Eyert V, Skibowski M, Friemelt K, Bucher E and Hüfner S 1996 *Phys. Rev.* B **54** 2453
[5] Perfetti L, Rojas C, Reginelli A, Gavioli L, Berger H, Margaritondo G, Grioni M, Gaál R, Forró L and Rullier Albenque F 2001 *Phys. Rev.* B **64** 115102
[6] Rossnagel K, Kipp L, Skibowski M, Solterbeck C, Strasser T, Schattke W, Voß D, Krüger P, Mazur A and Pollmann J 2001 *Phys. Rev.* B **63** 125104
[7] Rice T M and Scott G K 1975 *Phys. Rev. Lett.* **35** 120
[8] Wilson J A and Mahajan S 1977 *Commun. Phys.* **2** 23
[9] Pillo Th, Hayoz J, Berger H, Levy F, Schlapbach L and Aebi P 2000 *Phys. Rev.* B **61** 16213
[10] Hughes H P 1977 *J. Phys. C: Solid State Phys.* **10** L319
[11] Shimakawa M, Maki H, Nishihara H and Hayashi K 1997 *Mater. Res. Bull.* **32** 689
[12] Shimakawa M 1997 private communication
[13] Öhrwall G, Baltzer P and Bozek J 1999 *J. Phys. B: At. Mol. Opt. Phys.* **32** L51
[14] Zunger A and Freeman A J 1977 *Phys. Rev.* B **16** 906
[15] Wexler G and Woolley A M 1976 *J. Phys. C: Solid State Phys.* **9** 1185
[16] Voit J, Perfetti L, Zwick F, Berger H, Margaritondo G, Grüner G, Höchst H and Grioni M 2000 *Science* **290** 501
[17] Wells B O, Shen Z-X, Matsuura A, King D M, Kastner M A, Greven M and Birgeneau R J 1995 *Phys. Rev. Lett.* **74** 964
[18] Mott S N 1990 *Metal–Insulator Transitions* (London: Taylor and Francis)
[19] Zunger A and Freeman A J 1978 *Phys. Rev.* B **17** 1839
[20] de Boer D K G, van Bruggen C F, Bus G W, Coehoorn R, Hass C, Sawatzky G A, Myron H W, Norman D and Padmore H 1984 *Phys. Rev.* B **29** 6797
[21] Corcoran R, Meeson P, Onuki Y, Probst P-A, Springford M, Takita K, Harima H, Guo G Y and Gyorffy B L 1994 *J. Phys.: Condens. Matter* **6** 4479